Two-color Two-photon Rubidium Optical Clock with AC-Stark and Temperature Shift Suppression

Alexandra Plocki

A thesis submitted to the Faculty of the Honors Council of the University of Colorado in partial fulfillment of the requirements for the award of departmental honors in the Department of Physics 2024

This thesis entitled: Two-color Two-photon Rubidium Optical Clock with AC-Stark and Temperature Shift Suppression written by Alexandra Plocki has been approved for the Department of Physics

---

Professor Thomas Schibli

Department of Physics

Professor Paul Beale

Department of Physics

Professor Jonathan Wise

Department of Mathematics

The final copy of this thesis has been examined by the signatories, and we find that both the content and the form meet acceptable presentation standards of scholarly work in the above mentioned discipline.

Acknowledgments

Funding for my involvement was partially provided by the University of Colorado Boulder undergraduate research opportunity program. I am thankful that they saw my potential to conduct meaningful research. I want to thank my faculty mentor, Professor Thomas Schibli, for taking me on as a Sophomore and teaching me about the world of optical clocks. In addition to Prof. Schibli, I would like to thank the graduate student Nghia Tin Nguyen for guiding me through this project and for taking the time to teach me a lot of helpful information and skills.

Abstract

Navigation, positioning, and timing rely heavily on compact optical clocks. Warm vapor clocks utilize vapor cells near room temperature to maintain vapor pressure and thus do not require the complex cooling systems of cold atom clocks. Using the two-photon $5S_{1/2}$-$5D_{5/2}$ transition of rubidium with the $6P_{3/2}$used as an intermediate stage one-color clocks can typically reach fractional stabilities in the order of $10^{-12} - 10^{-15}$ at peak performance. We show the architecture for a two-color clock using the same transition with temperature and AC stark shift suppression that could significantly improve fractional stability over other rubidium time standards. Before implementing several sources of frequency shift, our clock reaches fractional stability of 10^{-12} at one second with some fluctuations at longer timescales.

Contents

1 Introduction

Positioning, navigation, and timing (PNT) rely heavily on precise time standards created by some of the most precise atomic clocks in the world. Although rubidium (Rb) clocks can not reach the levels of precision required for the most precise atomic clocks, which reach fractional instabilities in the order of 10^{-19} and are used for exploring fundamental physics [1], their performance and practicality, combine to make them some of the most useful innovations of the last 60 years [1], [2]. Cold atomic clocks achieve their exquisite stability with a single ion or many neutral atoms trapped in an optical lattice structure, requiring complex vacuum systems and laser cooling. Thus, they occupy cubic meters of space and are hard to maintain [1]. A stability around 10^{-15} is sufficient for PNT application; therefore, Rb clocks that are much easier to build and maintain are much better suited for several applications [2].

The two-photon $5S_{1/2}$-$5D_{5/2}$ transition of warm vapor Rb has long been considered as both a secondary representation of the second and an optical reference [3]. The setup is relatively simple due to the accessibility of the lasers to create the colors to interrogate the Rb and the lack of vacuum systems and laser cooling. Additionally, the Rb reference has a high atomic quality factor (Q factor) and is easy to use for 1550 nm telecommunication components using a frequency comb [3]. The Q factor measures the damping of a resonator's oscillations; an oscillator with a high Q factor will lose energy more slowly. Thus, the fractional line width is narrower compared to an oscillator with a lower Q factor. A narrower fractional linewidth translates to better fractional instability of the clock. Unfortunately, the methods that have been explored have several sources of systematic frequency shift. Frequency shift can be caused by any change in the cell temperature, the Rb pressure, the magnetic field, the laser power, and more. There are seemingly infinite factors to control when creating an optical clock. However, to create a time standard, the lasers must be locked to the atomic transition of Rb $5S_{1/2}$-$5D_{5/2}$ transition; thus, any change in any of those factors introduces instability or systematic error in the time standard. For instance, Clocks using the $5S_{1/2}$-$5D_{5/2}$ transition achieve fractional instabilities in the order of 10^{-13} to 10^{-15}

depending on the interrogation time scale [[3], [4], [5]]. This performance hardly demonstrates the potential of this transition. Issues arise when time scales are longer than 10 ks, as the aforementioned systematic errors affect the clock performance.

The scheme discussed in this thesis draws from two recently proposed schemes to improve the performance of Rb vapor clocks. Gerginov and Beloy proposed using a two-color scheme rather than the standard one-color scheme. The two colors are created by blue detuning one of the lasers by a few GHz from the $5S_{1/2}$-$5D_{5/2}$ transition to have two interrogating lasers of different colors [3]. The other scheme we draw from is that of Perrella et al., who uses a 1.5 GHz red detuning rather than a blue detuning to achieve frequency shift cancellation [6]. In contrast to both Gerginov and Beloy and Perrella et al., we implement both ac Stark and temperature shift suppression by choosing a specific combination of detuning, laser intensity, and cell temperature [1]

1.1 Thesis Outline

This thesis will begin with section 2, which details the background for optical frequency combs, rubidium as a source of precise time standards, and the one- and two-color techniques. Chapter 3 will describe the experimental realization of the two-color clock, including the circuitry and spectroscopy sections. In sections 4 and 5, the experiment's results will be presented. Finally, the conclusion will discuss the future of Rb clocks and the two color schemes.

2 Background and Literature Review

2.1 Optical Frequency comb

For our experiment, the frequency comb acts like the gears of an analog clock. It produces an optical spectrum of perfectly evenly spaced frequencies that enable the division of optical frequencies to microwave frequencies. John Hall and Theodor Hansch won the Nobel Prize in Physics in 2005 for their contributions to laser-based precision spectroscopy, including the frequency comb. Since its invention, it has become

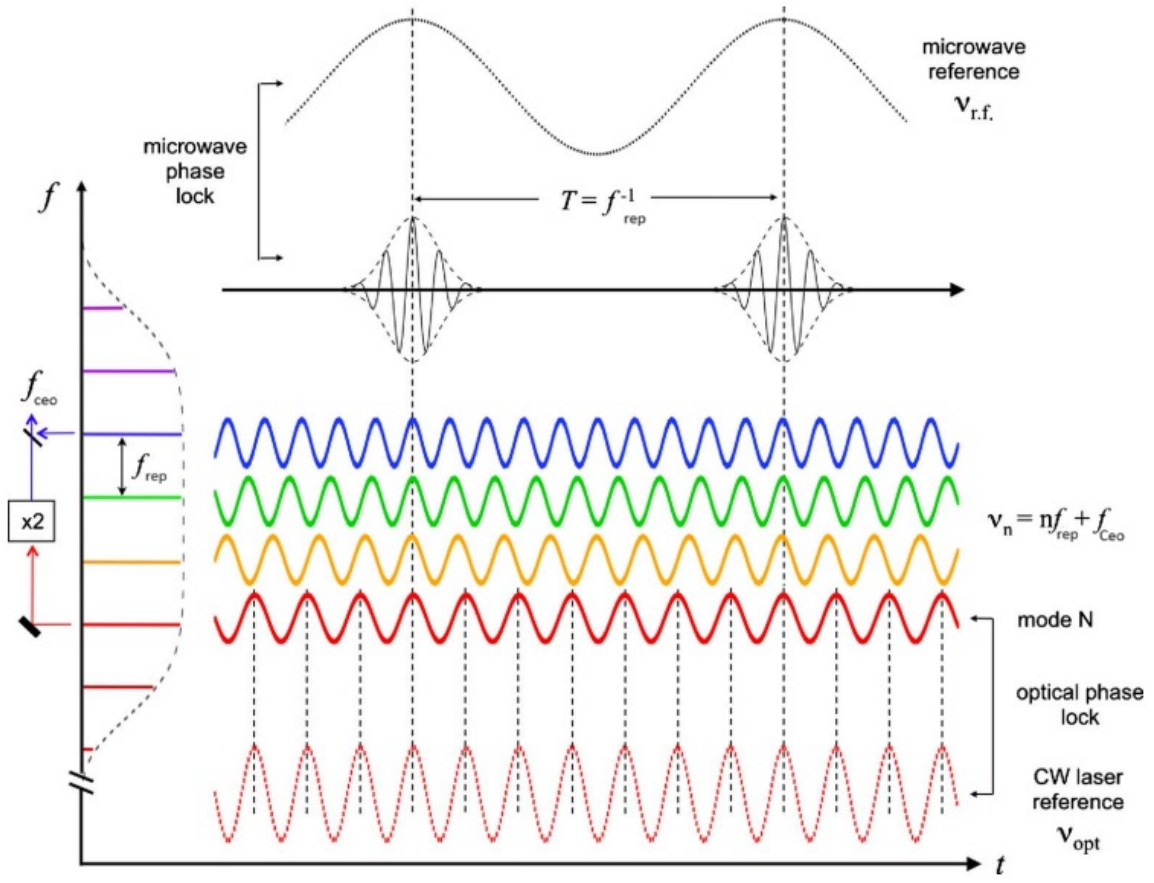

Figure 1: Time-frequency interpretation of the output of a mode-locked laser. The lines of the comb are similar to a series of cw lasers locked in phase that coherently add to create a short pulse with a period T, which is the inverse of the repetition rate (f_{rep}). Figure adapted from [7].

invaluable for countless applications. Optical frequency combs allow for far more precise manipulation of the optical spectrum and, thus, far more precise timekeeping.

The frequency comb used in this experiment is shown at the top of Figure 3. Once the comb is built, the repetition frequency (f_{rep}) and the carrier-envelope offset frequency (f_{ceo}) must be locked so that a reliable frequency reference can be established. f_{rep} determines the spacing between the lines of the spectrum, which can be seen in Figure 1. f_{ceo} is the offset of the whole frequency comb. Locking f_{ceo} allows the change in carrier envelope offset per resonator round trip $\Delta\phi_{ceo}$ to be constant; thus, all-optical line frequencies can be determined by

$$\nu_j = f_{ceo} + j \cdot f_{rep}, \tag{1}$$

where j is an integer index and

$$f_{ceo} = \frac{\Delta\phi_{ceo} mod 2\pi}{2\pi}\ f_{rep}. \tag{2}$$

Once the two frequencies are known, any arbitrary optical frequency in the comb range can be determined by measuring a beat note between the unknown frequency and the comb. This technique could also be used to phase lock a cw laser to one of the modes in a stabilized frequency comb. The basic idea of an optical phase lock is shown in Figure 1. It establishes coherence between the laser and the optical reference, allowing for precise control of the optical frequency produced by the laser. After locking the lasers to the frequency required to excite the atom, the frequency comb can be used again to measure the "ticks" of the atomic reference, which are at very high frequencies, into terahertz [8] and link them to the lower frequency "ticks" of microwave frequencies.

2.2 Rubidium

Rubidium has been investigated as a candidate for optical clocks since the 1990s, specifically the $5S_{1/2}$-$5D_{5/2}$ transition; however, it has been in use in the microwave domain since the 1950s [2], [9]. The use of Rb alleviates many of the difficulties that other atoms present. Atomic clocks can be built around many different atoms depending on the experiment's goal. Some of the most precise clocks in the world use strontium, cesium, ytterbium, and other atoms. Such clocks are highly precise, reaching fractional instabilities around 10^{-19}. Strontium clocks use a strontium transition around 695 nm, which can be difficult to produce. Such cold atomic clocks use highly complex systems to create a time standard. A common scheme uses ions or atoms trapped in an optical lattice [1]. Either way, these clocks require highly complex vacuum systems and lasers that are expensive and difficult to work with. Additionally, atoms in an optical lattice require laser cooling, further complicating the system. Although these clocks create an incredibly precise time standard, they typically take up large amounts of space and time to build and maintain. Additionally, the precision of that caliber is not needed for PNT applications. Rubidium, on the other hand, has none of those space

constraints. The warm vapor can be held in an aluminosilicate glass cell with magnetic shielding that can be held in one hand [1]. In addition to this, the transition has a high potential to create a precise time standard, although to a lesser degree than a cold ion or atomic clock, as the energy level structure of Rb can effectively drive a narrow-linewidth two-photon transition [6]. The $5S_{1/2}$-$5D_{5/2}$ transition of rubidium has been previously explored with frequency stability of 3×10^{-13} at up to 2000 seconds [10]. This initial exploration opened the door to further techniques to make compact, precise optical clocks based on the two-photon transition.

The transition most commonly used for two-color Rb optical clocks is the $5S_{1/2}$-$5D_{5/2}$ transition with the $6P_{3/2}$ as an intermediate state. This transition is doubly forbidden for single photons; however, it can be easily accessed using two photons thanks to the intermediate P state. The intermediate P state is a slightly off-resonant, dipole-allowed state. This allows for a significant excitation rate even at low optical intensities [8]. This transition also allows for easy detection of the excitation due to the cascade decay from $5D_{5/2}$-$6P_{3/2}$-$5S_{1/2}$; unfortunately, this also results in a broadening of the clock transition line width to about 334 kHz [6], [8]. Despite the broader transition line width, the remaining advantages make Rb an interesting candidate for further investigations as a source for precise time standards.

2.3 One-Color Scheme

State-of-the-art Rb vapor clocks utilize the aforementioned $5S_{1/2}$-$5D_{5/2}$ transition. One laser at 778.1 nm traverses the Rb cell, and it then doubles back through the cell, as shown in Figure 2. The atoms absorb photons from the counter-propagating beams, ensuring no Doppler broadening of the transition [11]. The atoms are excited to the $5D_{5/2}$ state, where they relax to the $6P_{3/2}$, releasing a photon outside the visible spectrum, from there they cascade down to the $5S_{1/2}$ state, releasing a blue photon at 420 nm wavelength. The fluorescence (blue photon) from Rb can be weak; thus, a photo-multiplier tube (PMT) is required to detect it as they can detect single photons. The 778 nm laser is tuned to match exactly with half the transition frequency of the Rb

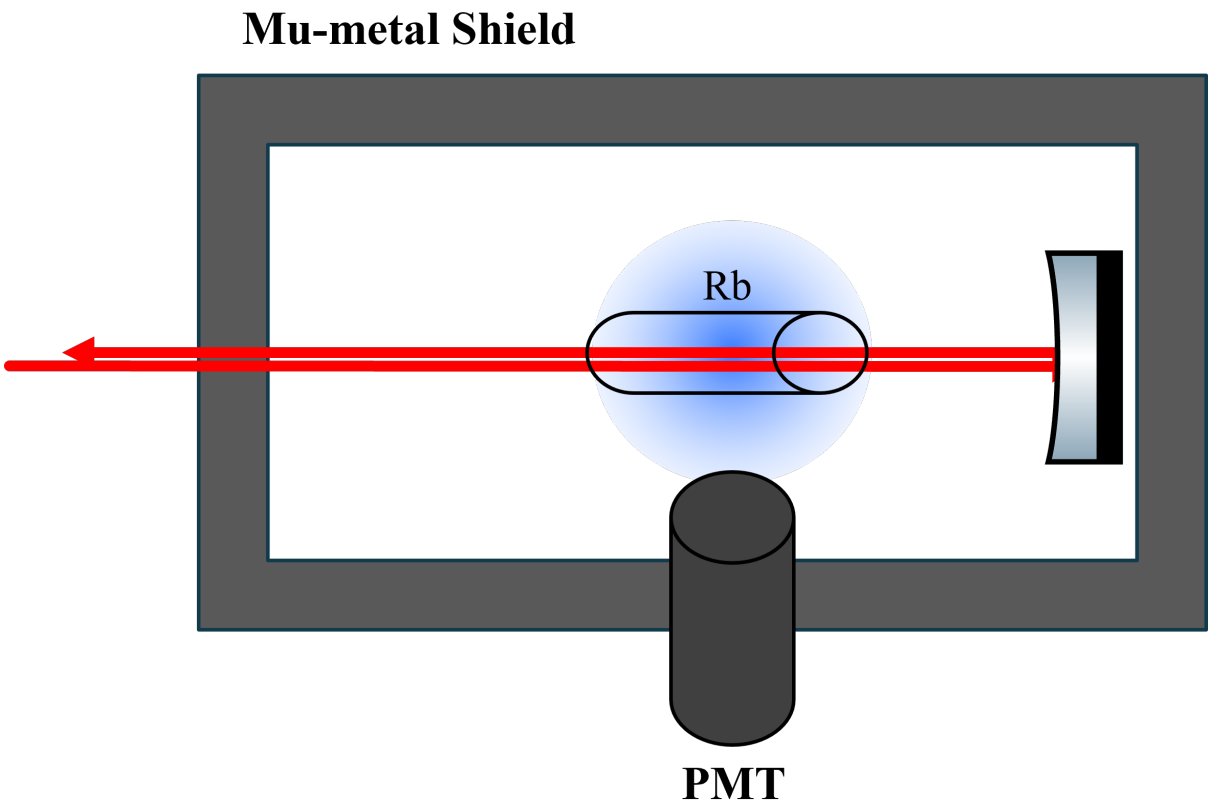

Figure 2: Very basic example of an Rb vapor cell used in one-color clocks with mu-metal shielding to reduce spectral broadening associated with the Zeeman shift and to protect the cell from low-frequency and static magnetic fields [8].

(778.1 nm) so that the counter-propagating beam excites the atom. A common source for this frequency is frequency-doubled light from a telecom erbium fiber laser at 1556.2 nm. This is a readily available commercial laser with ultra-low phase noise and low-intensity noise with laser line widths narrower than 1 kHz (Koheras BASIK). Using such lasers ensures a significant signal-to-noise ratio (SNR) so that one color clock can achieve fractional instabilities better than 10^{-13} from 1-10,000 s [4].

Improving beyond a stability of 10^{-13} requires mitigation of several sources of frequency shift. Zeeman shift and helium collisional shift are the easiest to mitigate. The Zeeman shift is analogous to the Stark shift but for a magnetic rather than an electric field, and the helium collisional shift occurs when helium infiltrates the rubidium cell, broadening the transition lines and contributing to a frequency shift [1]. These sources of shift can be prevented by implementing properly demagnetized multilayer magnetic shields and a Rb cell made of aluminosilicate glass [1]. With those

improvements, a fractional instability could be achieved in the order of 10^{-15}. However, Stark and temperature-induced shifts require precise laser power control to microwatt power fluctuations and a cell temperature stabilization to sub-millikelvin temperature fluctuations over a 1-day average time [8]. Due to these technical limitations, fully realizing a Rb optical clock with the one-color scheme would require sacrificing the size, weight, and power benefits Rb vapor clocks offer.

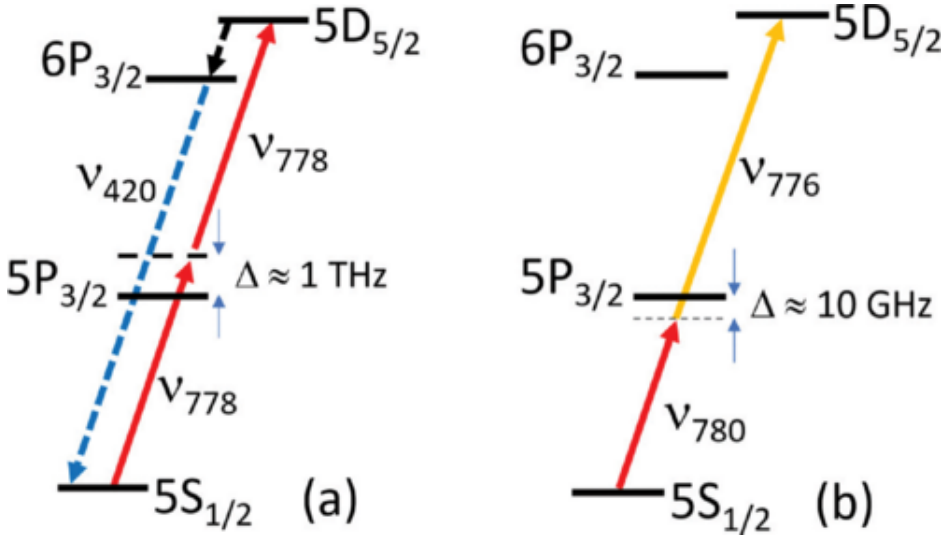

Figure 3: Two-photon . (a) Traditional two-photon excitation with a single color. The blue fluorescence from the dipole-allowed decay chain is typically used as an error signal to tune the value of ν_{778}. (b) Two-color, two-photon transition between the same levels. Tuning one of the two colors slightly below the $5P_{3/2}$ transition allows tuning the transition phase to effectively suppress the ac Stark and the temperature shift effects. Figure adapted from [1]

2.4 Two-Color Scheme

Although the difference between the one and the two color schemes can seem trivial, using two laser beams of different frequencies can greatly increase the stability of the clock compared to the one color scheme. This scheme was first proposed by Gerginov and Beloy and by Perrella et al. as an alternative to the one-color scheme [3], [6]. Figure 3 shows the difference in how the two beams excite the Rb compared with the one beam from the one-color scheme. One beam is detuned from the intermediate $5P_{3/5}$ state by a much smaller amount than in the one color scheme. The scheme was designed to cancel ac Stark shift by taking advantage of the sign of polarizability

between the 780 and 776 nm excitation pathways and by maintaining the correct ratio between the beam intensities [1]. The intensity ratio that allows for complete cancelation of the ac stark shift is given by,

$$\frac{I_{780}}{I_{776}} = (0.0656)[1 - (8.06 * 10^{-3})\Delta - (3.19 * 10^{-6})\Delta^2], \tag{3}$$

where I_{780} and I_{776} are the intensities of the 780 and 776 nm laser beams, respectively, and Δ is the detuning of the 780 nm laser relative to the intermediate $5P_{3/2}$ level [1], [3]. Unfortunately, the use of two different colors means the Doppler effect can not be fully suppressed, resulting in the transition line shape taking on a Voigt profile and a shift of the line center [1], [12]. This change in the line center leads to residual Doppler broadening of the transition line of a few MHz at 90°C [6] and a residual Doppler shift given by,

$$\nu_{780} + \nu_{776} - \nu_{fg} \approx \frac{1}{4ln2}(\frac{\nu_{780} - \nu_{776})\nu_{780}(\bar{v}/c)}{\nu_{780} - \nu_{ig}}, \tag{4}$$

where ν_{780} and ν_{776} are the frequencies of the 780 and 776 nm lasers, respectively, ν_{fg} is the natural transition frequency between the ground state $5S_{1/2}$ and the excited state $5D_{5/2}$, while ν_{ig} is the transition frequency between the ground state $5S_{3/2}$ and the intermediate state $5P_{3/2}$ [1]. $\bar{v} = \sqrt{8k_BTln2/m}$ is proportional to the average speed of the atoms, with k_B being the Boltzmann constant, T being the absolute temperature of the atoms, and m being the mass, for large detunings of the 780-nm laser from the intermediate level, of a Rb atom for [1]. The pulling effect will be proportional to $\bar{v}$ and T with its sign depending on the difference between ν_{780} and ν_{ig}. It will be strongest for smaller detunings of the 780 laser [6].

In Perrela et al.'s scheme, the 780 nm laser is red-detuned by 1.5 GHz from the intermediate state in order to cancel some of the Rb-Rb coalitional shift. However, due to the slight detuning, the pulling effect outweighs the collisional shift at low temperatures [1]. Greginov and Beloy proposed a 10 GHz blue detuning from the intermediate transition. This larger detuning results in less pulling effect than Perrela

et al.'s scheme; however, the cell temperature's long-term stability limits the clock's long-term stability [1]. Both these schemes utilize ac Stark shift cancellation but encounter issues with temperature-induced frequency shifts. However, if ac Stark and temperature-induced shifts can be canceled simultaneously, the stability of the two-color two-photon Rb clock would significantly increase.

The scheme used here is a realization of a scheme proposed by Nguyen and Schibli [1], which combines and modifies the schemes used by Greginov and Beloy and Perrela et al.. Similarly to Greginov and Beloy, we propose using the 10 GHz detuning for the intermediate P state, resulting in the pulling effect taking on the opposite sign of the Rb-Rb collisional shift and black body radiation. Black body radiation is electromagnetic radiation emitted by all bodies above 0 K and exists over all wavelengths. The higher detuning of form the intermediate state allows for a lower cell temperature than the Perrela et al. while using the pulling effect to suppress the Rb collisional shift. We operate the cell around the optimal temperature of 79.5°C, which is found by calculating the local maximum in temperature-induced shifts [1]. At this temperature, the clock's frequency dependence on temperature is given by $\Delta\nu = a(T - T_{opt})^2$ where a is the second-order temperature coefficient, which is dependent on the detuning [1]. The 10 GHz detuning used in this study takes on a value of -6.12 Hz/K^2, meaning for a temperature drift within 100 mK, the contribution to fractional instability is only 8×10^{-18}, which is much lower than what has been achieved by one or two color clocks to date [1]. The dependence of optimal temperature on the detuning is resolved by generating a 10 GHz sideband from the 780 nm probe laser and locking it to the transition. The combination of ac Stark shift cancellation and temperature shift cancellation could result in a two-color Rb clock that far outperforms any Rb clock available to date.

2.5 Modulation Transfer Spectroscopy

Modulation transfer spectroscopy (MTS) is a technique for sub-Doppler spectroscopy where an atomic transition is used to transfer modulation from a pump

beam to a probe beam. We use this to transfer modulation sidebands around the ν_{776} pump beam to the ν_{780} probe beam via the atomic transition of Rb in order to determine the exact transition frequency at $\nu_{776} + \nu_{780}$. The counterpropagating pump and probe beam are shown in Figure 4. The pump beam, which has a frequency ν_{776}, is frequency-modulated with a modulation frequency of $\Omega = 650kHz$, and the probe beam is not modulated [13]. As the atoms oscillate between the ground and excited states, the state population transfers modulation from the pump beam to the probe beam [13], [14]. After transmitting through the cell, the probe beam will be phase-modulated with a frequency of Ω. MTS has many advantages over other sub-Doppler spectroscopy techniques, such as Saturated Absorption Spectroscopy (SAS), Polarization spectroscopy (PM), Frequency Modulation Transfer spectroscopy (FMT), etc., because MTS is not affected by environmental conditions such as temperature and its ability to provide robust laser frequency stabilization [13].

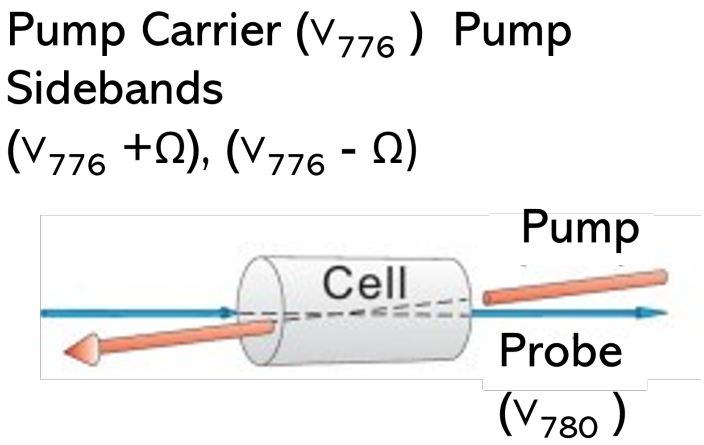

Figure 4: Diagram of the beam path for modulation transfer spectroscopy. Figure adapted from [13]

3 Methods

3.1 Experimental Realisation

The experiment can be divided into three sections: the optical clockwork shown in Figure 5 (bottom), the locking circuitry, and the frequency comb shown in Figure 5

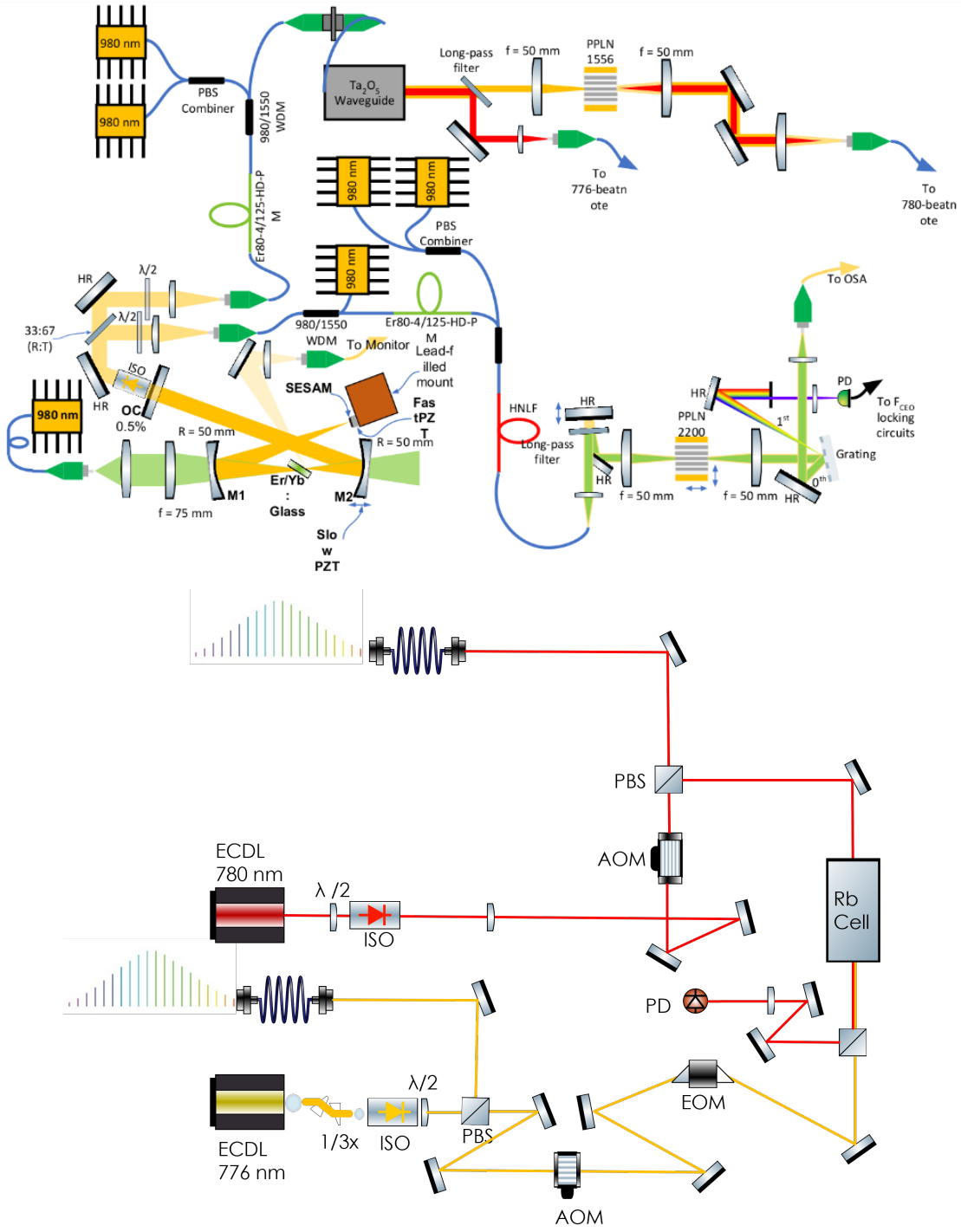

Figure 5: Schematic of the Frequency comb (top) and the optical clockwork (bottom). Electro-optical modulator (EOM), acousto-optical modulator (AOM), isolator (ISO), external cavity diode laser (ECLD), photodiode (PD), polarization beam splitter (PBS), semiconductor saturable absorber mirror (SESAM), lead zirconate titanate (PZT), periodically poled lithium niobate (PPLN), highly nonlinear fiber (HNLF), wavelength division multiplexing (WDM)

(top). The clocks work by locking the lasers to the atoms' excitation frequency so that the atoms are excited most effectively. Each beam is split using a beam splitter. A portion is directed to the locking circuitry, and the other portion is directed to the Rb cell, where the atoms will be excited. After the 780 nm (red in Figure 5) beam traverses the cell, it is directed into a silicon photodiode, where the modulation transfer from the pump beam to the probe beam is measured to create a precise time standard. However, the general idea of how the clock works can seem quite simple, and properly executing the setup can be quite complicated.

3.1.1 Spectroscopy

The optics consist of two tracks in order to achieve properly prepared counterpropagating beams. One track is for the 776nm laser (Yellow in Figure 5), and the other is for the 780 nm laser (red in Figure 5). An image of the physical setup can be seen in Appendix 1. Immediately after exiting the laser, the 776 nm beam transmits through a 3.0x anamorphic prism pair to shape the beam into a circular beam profile. When the beam exits the laser, it has a slightly elliptical shape. The anamorphic prism pair shapes the beam with a tighter circular cross-section. Following the anamorphic prism pair, the beam is transmitted through an isolator to ensure that no light is sent back into the laser diode, which would damage it. Subsequently, the beam traverses a beam splitter, which divides the beam so a portion continues to the rest of the setup, and the other portion is redirected into the frequency comb. The portion that continues to the Rb cell transmits through an acousto-optical modulator (AOM). This AOM will be used for residual amplitude modulation (RAM) suppression. RAM arises from imperfect phase modulation of the laser beam [15]. However, RAM suppression was not employed during this study as it is not required to implement the AC Stark and temperature suppression scheme. Next, the beam is transmitted through an electro-optical modulator (EOM). An EOM uses an electrical signal to modulate a laser's power, phase, or polarization. In this instance, a QUBIG model PM6-VIS 0.65 EOM is used as a phase modulator to generate a pair of sidebands around the CW

laser, which is necessary for the modulation transfer technique. Although much of the setup was already in place, the section where the beam is redirected to the frequency comb through an optical fiber was incomplete. Figure three shows that the free space beam must be coupled into the fiber to combine the optical signal from the comb and lasers for locking.

The 780 nm laser follows a similar path to the 776 nm laser. However, unlike the 776 nm laser, the 780 nm laser has an anamorphic prism-pair inside the device, so an external one is not required; rather, the beam goes directly through an optical isolator. After the isolator, the beam is directed into a model 3080-122 Crystal Technology AOM. An AOM is a device that can modulate the power of a laser by modifying the refractive index of a crystal or glass using sound waves. One beam enters the AOM, and two beams, the zeroth and first-order diffracted beams, exit at different angles. This setup uses the zeroth-order un-diffracted beam with its intensity modulated by the change in RF intensity, which changes the crystal's refractive index. This is necessary for the AC stark suppression scheme because it allows us to check the suppression of the ac Stark effect. Following the AOM, the beam is transmitted through a beam splitter where a portion of the beam is redirected for locking, and the rest continues to the Rb cell. Once at the Rb cell, both beams are aligned to counterpropagate and perfectly overlap in space. Even a slight angle between the beams can cause a frequency shift. The counterpropagating beams excite the Rb. After the modulated 780 nm beam transmits through the Rb cell, it is directed onto a silicon photodiode (Hamamatsu S5972).

The key to this scheme is to properly align the counter-propagating beams to interrogate the Rb atoms. The lab environment can drastically impact the alignment of the optics. Small temperature and humidity changes can cause the precisely aligned optics to drift over time, changing the beam path and introducing a residual Doppler shift. When the optics become misaligned, the function of the clock will cease. Initially, the entire clock set up was sitting on the table exposed to the lab air, so it was susceptible to changes in the lab environment. However, the setup has since been transferred into a thick plastic box, as seen in the image of the final physical setup in

Appendix 2. The box protects the setup from small temperature changes and can prevent large amounts of drifting if the lab temperature control is interrupted. In addition to the effect on the optics, the lab environment affects the clock's stability. Therefore, moving it into a box can mitigate temperature changes and vibration, which both can have a noticeable effect on the clock's performance.

3.1.2 Generating the Carrier Envelope offset Frequency

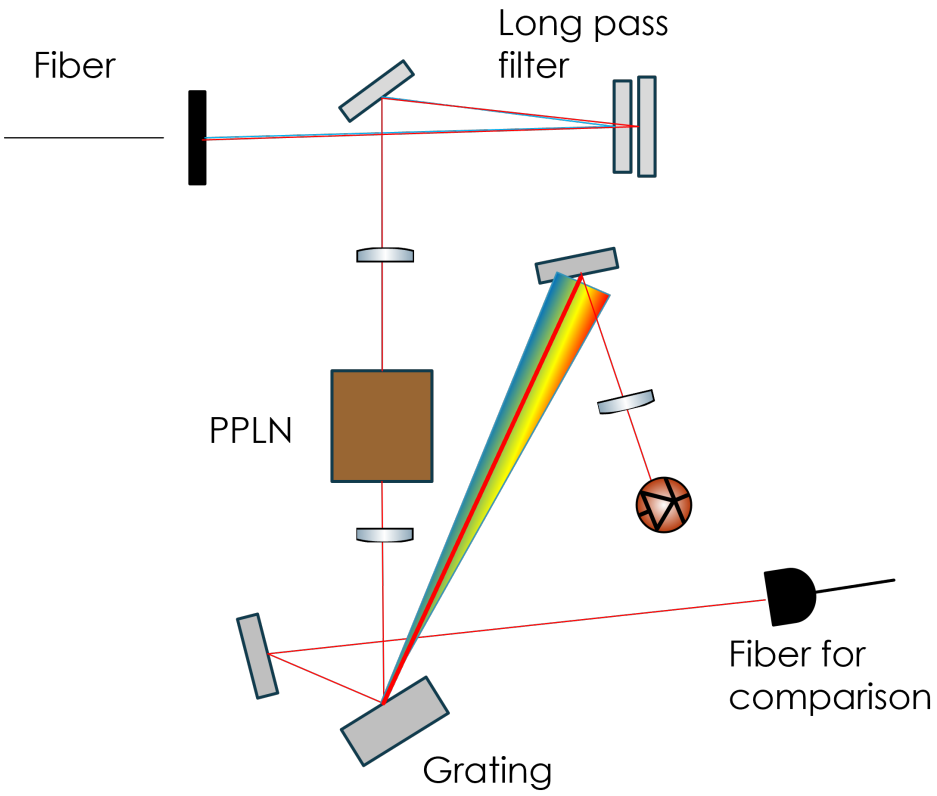

Figure 6: Setup for carrier-envelope offset frequency generation. Light enters the setup through a highly nonlinear fiber. A supercontinuum is generated and used to lock the carrier-envelope offset frequency of the comb.

A crucial part of building a comb that creates consistent, perfectly spaced comb lines is detecting and locking f_{ceo}. The experimental setup for locking f_{ceo} is shown in Figure 6. The physical setup can be seen in Appendix 3. The entire setup is inside a plastic box separate from the comb and the spectroscopy. Comb light enters the setup on the top through a highly non-linear fiber. Due to the different speeds between the low and high frequencies of the light, the laser pulses disperse while traveling through

the fiber. To eliminate this dispersion, we arrange two mirrors so that the path of the faster wavelengths is longer than that of the slower wavelengths. We need to eliminate the dispersion so that the two beams match in frequency and time. Once this is complete, we interfere with the two beams as they transmit through a periodically poled lithium niobate (PPLN). A PPLN is a material that is used for nonlinear wavelength conversion processes. Here, it is used to double the frequency when the two photons from the two beams combine into a third photon. This creates a concentrated beam of a specific frequency within the supercontinuum, as seen in Figure 6. The beam is directed to a grating where some light is coupled into fiber for modeling on a spectrum analyzer. A photodiode detects the rest, and the signal is sent to the comb. This generates a beat note between the higher-frequency end and the frequency-doubled low-frequency end of the comb spectrum by generating an octave-spanning supercontinuum between them. The PPLN causes a peak at the beginning of the supercontinuum as a reference.

3.2 Phase Lock Circuitry

Locking the laser to the frequency required to excite the atoms is what allows the clock to work. By ensuring the lasers produce only a single frequency of light, we can ensure that only the desired transition of Rb is excited. In this case, we are locking the lasers used to interrogate the atoms to the optical reference created by a frequency comb. This experiment uses a heterodyne phase lock, which locks the phase evolution between the optical carrier of the cw and the frequency comb light. The basic loop required for a heterodyne phase lock is shown in Figure 7. The frequency comb lines create a reference for the cw laser, and coherence can be established between them as described in section 1.1. The light from the comb and the redirected light from each laser are combined, creating a beat note at the desired frequency. Any other beat caused by the comb can be filtered out, leaving only the desired frequency. When the two beams are combined, the new beam is a superposition of the two beams. The current in the photodetector is proportional to $|E|^2$, which is the amplitude of the incoming beam. The signal from the lasers, which now contains information about both

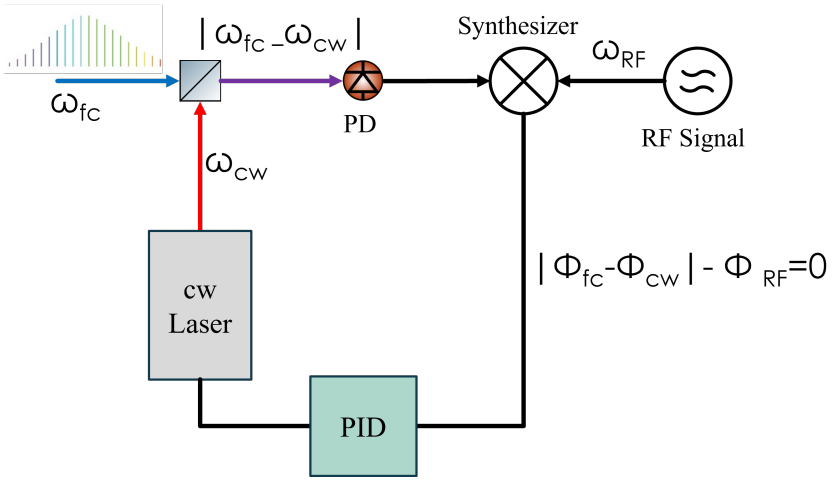

Figure 7: Basic diagram of a heterodyne phase lock with a cw laser and a frequency comb where ω_{fc} is the frequency from a line of the frequency comb, ω_{cw} is the frequency of the cw laser and ω_{RF} is a radio frequency for comparison. This comparison results in a phase lock between the two frequencies that are controlled by a proportional integral derivative controller (PID) and fed back into the cw laser.

original frequency ω_{fc} and ω_{cw}, and the phase difference $\Delta\phi$ is combined via a synthesizer with an RF signal ω_{RF}. A heterodyne phase lock uses the difference between $|\omega_{fc} - \omega_{cw}|$ and ω_{RF} to find the phase difference between the two original beams. The phase difference $\Delta\phi$ is proportional to the voltage. That signal is then controlled using a proportional-integrator-differentiator (PID) and fed back into the cw laser to control its frequency. This process requires electronics to control the error signal created when mixing the two sources to achieve the desired phase coherence between ω_1 and ω_2.

In our study, we mix the comb light and cw laser light in a fiber and then send the light into the photodetector. The detected signal then goes through three stages of amplification. After amplification, the signals are sent into a PID controller. A PID is a very common type of circuit that creates a loop to force feedback to match the setpoint of a system by detecting errors. The basic design of a PID is shown in Figure 8. It does this by continuously calculating error as the difference between the signal and a set point and then using the proportional integral and derivative terms to apply corrections. The proportional term controls how much feedback to use and is proportional to the error. the integral term pushed the signal based on accumulated error. The derivative term is proportional to the speed of the error and optimizes the

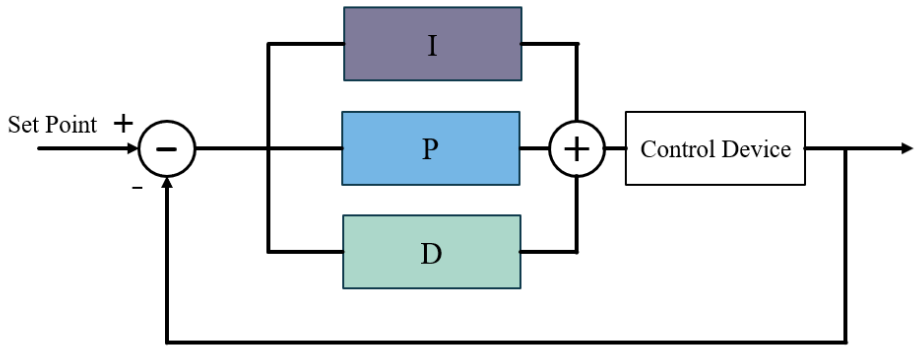

Figure 8: PID block diagram.

response time. These terms work together to adjust the signal to ensure it stays as close to the setpoint as possible. In this system, the signal detected is the difference between the comb and cw frequencies and an RF signal at 90 and 80 MHz for the 780 and 776 lasers, respectively. This process creates the heterodyne phase lock and forces the frequency of the cw laser to have a particular phase in relation to the comb line through a lead zirconate titanate (PZT) control loop and current modulation, which controls the laser crystal and the current to the laser respectively. We use a fast and slow PID to ensure the lock can be maintained for long periods of time.

The final PID this system uses has many advantages compared to the original loop filter. It saves space by combining several circuits into one, but most importantly, the new circuit design eliminated the parasitic phase lag that the previous design had. This caused the PID to be too slow to keep the phase lock. With the previous, a separate board was needed for the slow and fast PIDs on the 780 nm loop in addition to a supplementary PI circuit and the PZT feedback circuit. The new circuit contains all the extra components and performs much better than the original circuit design.

Once the PIDs lock the lasers to their respective frequencies, the signal feeds back into the lasers to modulate the current at high bandwidths and the PZT at low bandwidths. Each laser has also been supplemented with a fast current modulation circuit that allows the frequency of the laser to be changed based on the signal from the PID. After all the locking circuitry is implemented, the PID settings are chosen to achieve a stable lock. Many things can cause a phase lock to break, such as vibrations

in the room caused by lab activities. To ensure that the lock is robust and will last, SNR must be high enough that spikes in the noise will not cause the lock to break. Typically, 40 dB at 100 kHz bandwidth will ensure a lasting lock.

4 Results

Each step described above produces results that need to be monitored and perfected before moving on to the next step. Ensuring the PIDs work properly is paramount to achieving a robust phase lock. After implementing the PIDs, we monitor the lock on the 776 nm and 780 nm lasers as well as the f_{ceo} lock. This allows us to determine what changes to the system are needed to improve the clock's performance. Finally, we can measure the clock stability through the Allan deviation, which is the square root of the Allan variance. Allan variance is defined as one-half of the time average of the squares of the differences between successive readings of the frequency deviation sampled over the sampling period [16]. It is a function of the sampling period, and a lower Allan variance indicates a clock with good stability over that period [16]. Allan deviation is the criteria for determining the fractional instability of a clock, and comparisons can be made between several time standards.

4.1 PID results

When building a PID, it is important to ensure that it provides the proper frequency response for the application. PIDs are characterized by their frequency-dependent gain, which is the ratio between the output and input voltage. The integral gain decreases as a function of frequency. Once the gain of the integrator overlaps with the proportional gain, the proportional term begins to control the system. Once the proportional gain intersects with the derivative gain at high frequencies, the derivative term controls the system. The derivative gain increases as a function of frequency. These changes in the control terms are called corners'. Figures 9 and 10 show the frequency response of the original PID and that of the new PID, respectively.

The new PID provides better results for the phase for several reasons. With the new PID, the 776 and the 780 nm lock are controlled with similar setups; thus, only one design for the PID is needed. With the new PID design, the low-frequency gain is no longer capped at 40 dB at 4 MHz but rather increases to the gain-bandwidth limit of the operational amplifier used ($\approx$ 50 dB). The proportional section was largely unchanged, but the maximum high-frequency gain of the differentiator was greatly increased. The original PID provided less than 20 dB of gain at high frequencies, and the new one provided around 35 dB. The increased gains of the integrator and the differentiator results in better phase lock control. The increased gain of the integrator and differentiator combined with the lower phase lag results in a more robust phase lock with less residual phase noise.

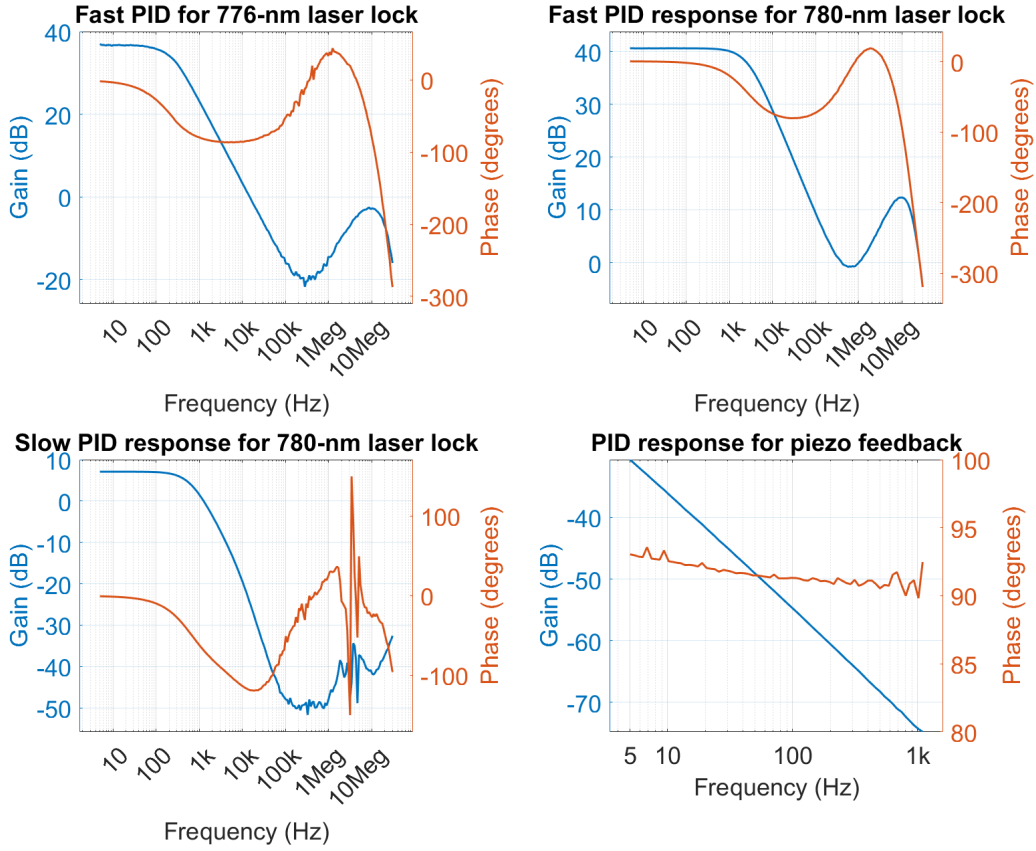

Figure 9: Frequency response of the original loop filters.

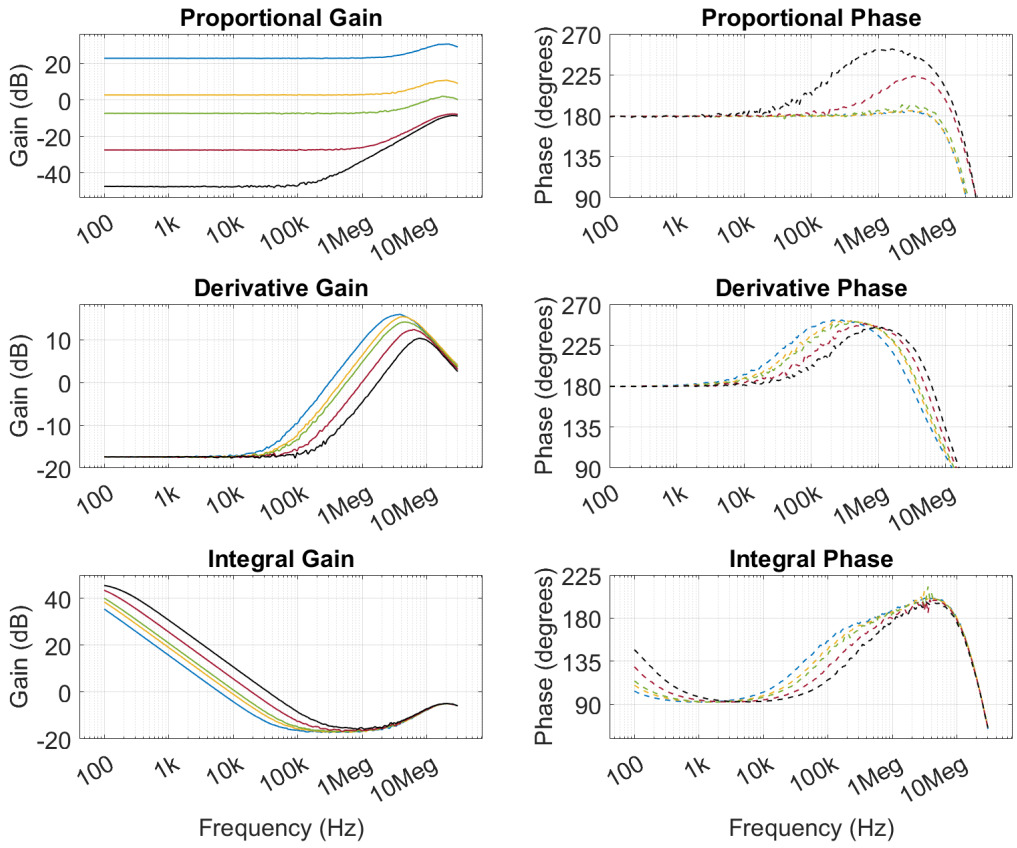

Figure 10: Frequency response for the new loop filters. On the left, from top to bottom, are the proportional, derivative, and integrator gains. On the right is the proportional, derivative, and integrator phase. The line colors represent different corner settings from low (black) to high (blue).

4.2 Locking Results

4.2.1 Locking the carrier-envelope offset frequency

In the process of locking f_{ceo}, we created the supercontinuum between the lowest and highest frequencies of the comb, as discussed above. In addition to the supercontinuum, we generated the PPLN peak. The PPLN peak is a peak in the power spectral density originally from doubling the low-frequency end of the supercontinuum to generate f_{ceo}. This is done by changing the current of the pumping lasers. This is visualized in Figure 6 by the strong beam in the center of the supercontinuum and the graphs in Appendix 3. Once both the supercontinuum and PPNL peak were generated, we adjusted the frequency of the PPLN peak so that it lined up with the short

wavelength edge of the supercontinuum in order to provide a reference for f_{ceo}. The graphs showing all three stages of this process are shown in Appendix 3. Once the supercontinuum is generated and stabilized, f_{ceo} can be locked to the desired frequency shown in Figure 11a. This lock has an SNR of around 50 dB at 1 kHz resolution bandwidth (RBW), allowing it to stay locked indefinitely. Figure 11b shows the residual phase noise of this lock. The first bump arises because there is still insufficient gain at low frequencies, and the second bump around 60 kHz is a servo bump. A servo bump is when the effective servo gain is reduced as phase shift increases to 90° and the servo fails to suppress noise. This servo bump is caused by the loop phase lag due to the finite response time of the laser gain and the loop filter parasitic phase lag. At high frequencies, the noise approaches the nose floor of the f_{ceo} beat note.

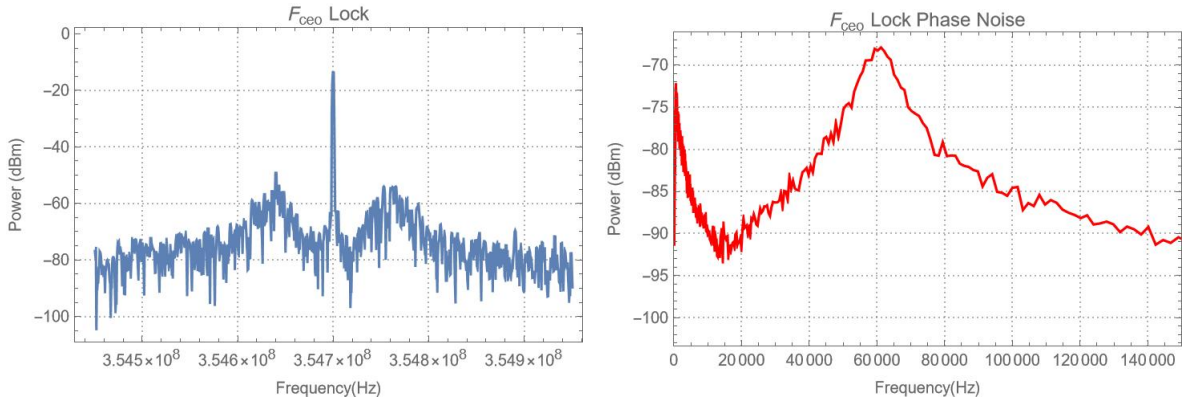

(a) (b)

Figure 11: On the left (a) is the frequency lock for the carrier-envelope offset frequency at 1 kHz residual bandwidth with. On the right (b) is the Phase noise for the carrier-envelope offset lock.

4.2.2 Phase locking the 776 and 780 nm lasers

As discussed earlier, phase locking is imperative to creating functional time standards. The free-running cw lasers will generally produce a fluctuating optical frequency with rapid fluctuations of up to 10 MHz, as seen in Figure 12. Comparing the free-running laser in Figure 12 to the phase-locked lasers in Figure 13, it is evident that the laser produces light at a single frequency of approximately 386 THz (776 nm). The locked laser has an SNR of around 35 dB at 100 kHz RBW. High SNR is required to

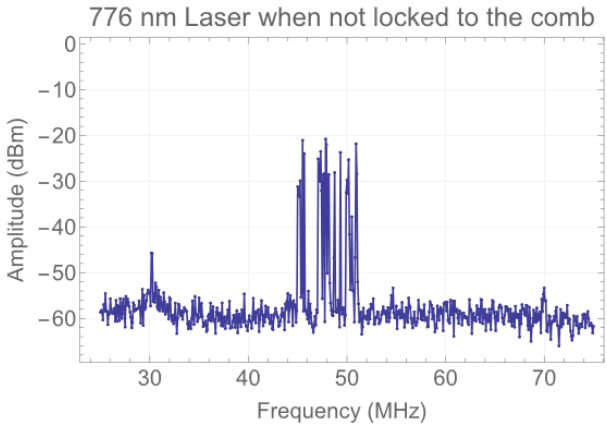

Figure 12: Frequency and power of the free-running 776 nm laser using the original experimental setup

maintain the lock because it prevents spikes in the noise from surpassing the phase margin of the phase detector used to lock the heterodyne beat note to the radio frequency reference. This would cause the lock to break or lead to phase shifts of multiples of 2π. 35 dB at 100 kHz is insufficient to maintain the lock for long periods of time or prevent cycle slipping. Cycle slipping is like the gears of the clock physically slipping, which disrupts the time standard. Because the SNR was rather low, we changed to the new PID to increase the SNR to approximately 45 dB at 100 kHz.

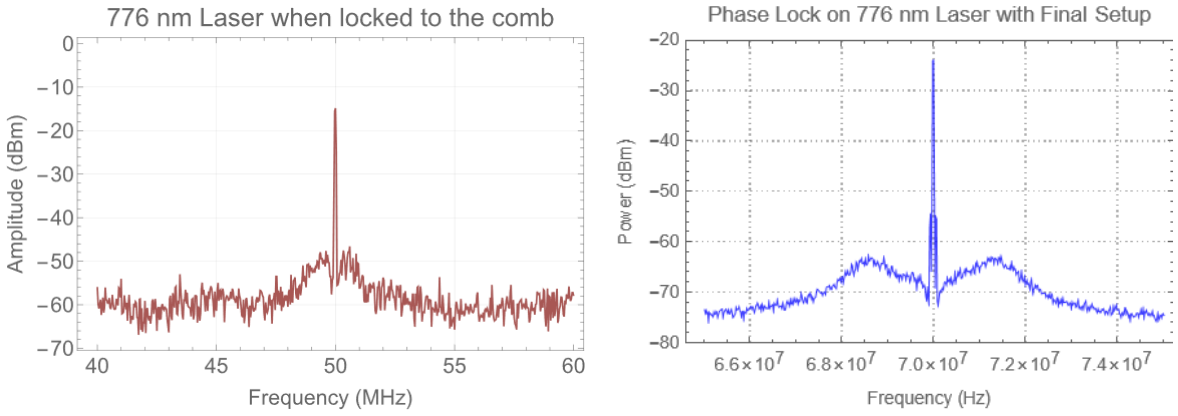

(a) (b)

Figure 13: On the left (a) is the frequency vs power of the phase-locked 776 nm laser using the original experimental setup at 100 kHz RBW. On the right (b) is the Frequency vs power of the phase-locked 776 nm laser using the final experimental setup at 100 kHz RBW.

The data presented in Figure 13a was taken with the original PID design and the original experimental setup with the spectroscopy sections on a breadboard that was

exposed to the lab environments. Figure 13b shows the new lock for the 776 nm laser after making the experimental adjustments described above. This graph shows that the improvements made to the experimental setup resulted in improvements to the lock of the cw lasers to the comb. Because the phase lock on the lasers is so much more robust, it should last indefinitely, providing that normal lab conditions are maintained. With a robust lock established, a consistent spectrum can be monitored from the Rb, and a time standard can be established.

4.2.3 Rubidum Atomic Spectrum

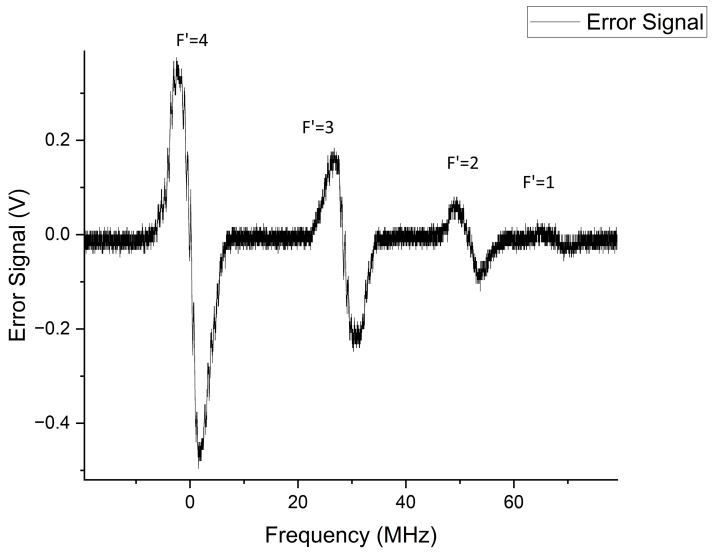

Figure 14: Frequency modulated spectrum of the $5S_{1/2}$,F=3 to the $5D_{5/2}$, F'=1,2,3,4 transition of ^{85}Rb used to lock the 776 and 780 nm lasers.

Using MTS, we can observe the Rb spectrum by detecting the modulated intensity of the 780 nm beam using a silicon photodetector. Figure 14 shows the spectrum of the $5S_{1/2}$-$5D_{5/2}$ transition of ^{85}Rb that the 776 and 780 nm lasers are locked. As discussed before, this method allows for better detection of the transition than using the fluorescence of the atom and at PMT. This data set was taken before f_{ceo} was stabilized, so the optical frequency comb was not locked and stabilized, which was thought to be the cause of the jagged lines throughout the spectrum. However, after locking f_{ceo}, the jaggedness was still present; thus, we believe it is due to the photodiode and amplifier

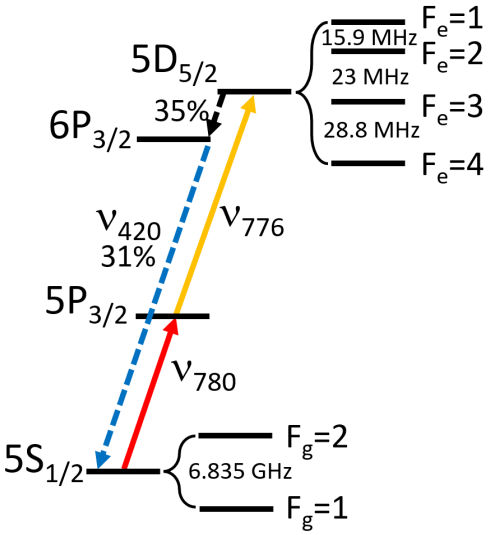

Figure 15: Two-color, two-photon transition between the same levels with angular momentum states of each energy level.

noise. Additionally, the RAM causes the spectrum to be asymmetrical. There are four transition peaks, although the fourth one is small and hidden by noise. The four peaks are a result of the F_g=2 to F_e=1,2,3,4 shown in Figure 15. There is also a F_g=1 to F_e=1,2,3 and two other ^{85}Rb transition groups that are not being used because they do not provide as clear of a transition. The peak-to-peak voltage of the largest transition is around .8 V, with the distance between the first peak and the subsequent peak being about 30 MHz. We use the zero crossing of this transition to lock the repetition rate of the comb, which finally allows us to compare the two-color clock to other precise time standards.

4.3 Comparison to a One-Color Rb Optical Clock

Once all four of the required phase locks (f_{ceo}, 776 nm, 780 nm, and f_{rep}) shown in Figure 16 have been achieved, the comb is stabilized, compare our clock to another precise time standard. Characterizing the time standard created by our two-color clocks can be done by creating a beat note between the two-color clocks and another time standard. In this case, we are comparing the two-color clock to a one-color, two-photon Rb optical clock. Figure 17a shows the beat note between these two standards, and Figure 17b shows the Allan deviation of that measurement. There is a large amount of

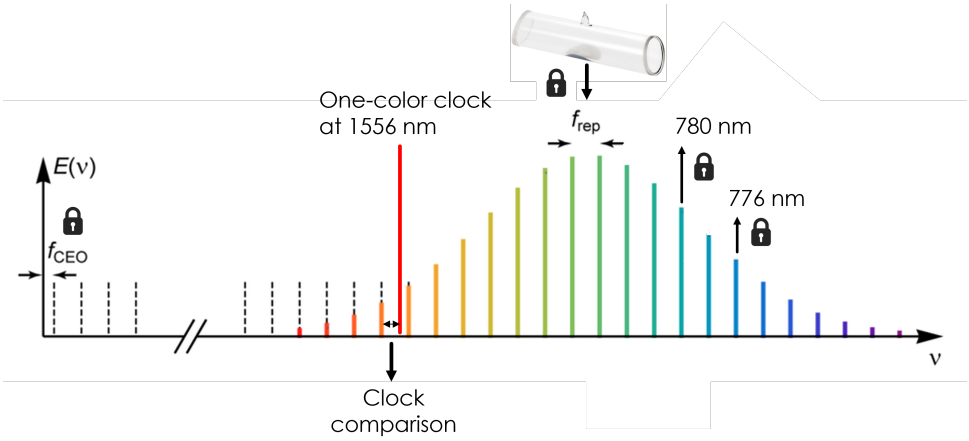

Figure 16: Diagram showing the lock of f_{ceo} the 776 nm and the 780 nm lasers to the comb and the locking of the comb repetition rate to the Rb transition. The red line represents the frequency of the one-color clock, and the difference between that frequency and a comb line is the clock comparison.

noise between the two standards and large amounts of deviation at timescales larger than 1000 s. The one-color clock that is being used as a comparison has a short-term fractional instability of $2.5 \times 10^{-13}/\sqrt{\tau}$ and is limited to 10^{-14} at timescales longer than 1000 s. Unlike the two-color clock, all RAM suppression, temperature control, and magnetic shielding of the Rb cell have been implemented in the one-color setup, meaning it operates at a much lower fractional instability compared to our device.

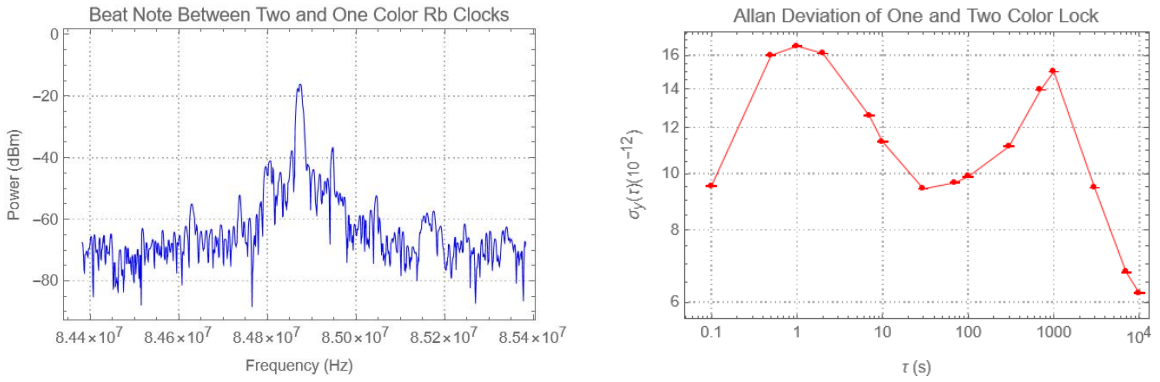

(a) (b)

Figure 17: On the left (a) is the beat note between a one-color Rb clock and the two-color Rb clock at 3 kHz RBW. On the right (b) is the Allan deviation of the beat note.

5 Discussion

Although the improvements made to the optical and circuitry components of the setup contributed substantially to stability improvements and the clock operation at larger time scales. The clock reached fractional frequency stability in the order of 10^{-11} for $1s < \tau < 1000s$. This is significantly worse than the one-color clock was compared, which has short-term fractional instability on the order of 10^{-13} at short time scales. For their two-color clock, Perreall et al. achieved fractional stability of 1.5×10^{-13} at integration times of 1 s and 4.9×10^{-14} at integration times around 100 s [6]. Several factors could cause the fluctuations in the fractional instability of the clock. The initial increase is likely due to the comb frequency being more stable than the frequency of the Rb atoms, thus decreasing the fractional stability. At longer time scales, the comb frequency becomes less stable due to thermal drifting, so the fractional stability improves as the atom's frequency becomes more stable than the comb's and the stability improves. The second spike shown in Figure 17b is likely due to the RAM introduced by the free-space EOM used to create the pair of sidebands. The thermal effect on the EOM causes RAM, which affects the spectrum produced by the Rb and, thus, the fractional stability of the clock. The RAM can be mitigated by replacing the free space EOM with one that introduces less RAM and implementing the RAM suppression scheme included in the setup but not used in this study. Further improvements to the stability can be made by implementing temperature control of the Rb cell to maintain the ideal temperature that was calculated for the 10 GHz detuning being used. Additional improvements can be made by building a properly demagnetized shield for the Rb cell, which will further protect it from its environment. If these improvements are made, this scheme could result in a frequency standard capable of fractional stability in the order of 10^{-15} at time scales of $\tau > 10$ks under ideal conditions.

6 Conclusion and Future Outlook

The two-color, two-photon Rb optical clock with ac Stark and temperature shift suppression has the potential to outperform the current generation of compact atomic clocks. While the results reached here do not immediately show the predicted fractional stability in the order of 10^{-15}, they demonstrate the potential of the scheme. Several systems imperative to creating precise time standards have not yet been implemented, such as the temperature control system that would keep the rubidium cell at the ideal temperature and RAM suppression. Although, at this stage in the study, the fractional stability is not comparable with previously published two-photon Rb time standards, the implementation of further standardization can improve the fractional stability.

Providing the execution of the above experimental refinements succeeds in showing the effectiveness of the scheme proposed here; there are many avenues to explore going forward. Maximizing the potential applications for such a time standard would require minimizing the size, weight, and power. This would focus on miniaturizing the system's architecture, including the locking electronics. Additionally, the locking electronics, including the temperature control system, would need to be automatized. Preparing the scheme for any space applications also requires engineering to overcome the radiation-induced darkening of the optical components that the optical clock would face in space [8]. These endeavors would provide a significant engineering challenge; however, implementing a time standard with fractional instability in the order of 10^{-15} would result in substantial improvements to a host of applications.

---

7 Work Cited

References

[1] Tin Nghia Nguyen and Thomas R. Schibli. "Temperature-shift-suppression scheme for two-photon two-color rubidium vapor clocks". In: *Phys. Rev. A* 106 (5

2022), p. 053104. DOI: 10.1103/PhysRevA.106.053104. URL: https://link.aps.org/doi/10.1103/PhysRevA.106.053104.

[2] William J Riley. "A history of the rubidium frequency standard". In: *IEEE UFFC-S History* (2019), p. 2.

[3] V Gerginov and K Beloy. "Two-photon Optical Frequency Reference with Active ac Stark Shift Cancellation". In: 014031 (2018), pp. 1–8. DOI: 10.1103/PhysRevApplied.10.014031.

[4] Matthew S. Bigelow et al. "A High Performance Clock Laser for Two-Photon Frequency Stabilized Optical Clocks". In: *Conference on Lasers and Electro-Optics*. Optica Publishing Group, 2018, JW2A.163. DOI: 10.1364/CLEO_AT.2018.JW2A.163. URL: https://opg.optica.org/abstract.cfm?URI=CLEO_AT-2018-JW2A.163.

[5] Gretchen Phelps et al. "Compact Optical Clock with 5×10^{-13} Instability at 1 s". In: *Navigation, Journal of the Institute of Navigation* 65.1 (2018), pp. 49–54. ISSN: 00281522. DOI: 10.1002/navi.215.

[6] C. Perrella et al. "Dichroic Two-Photon Rubidium Frequency Standard". In: *Phys. Rev. Applied* 12 (5 2019), p. 054063. DOI: 10.1103/PhysRevApplied.12.054063. URL: https://link.aps.org/doi/10.1103/PhysRevApplied.12.054063.

[7] Scott A Diddams. "The evolving optical frequency comb". In: *JOSA B* 27.11 (2010), B51–B62.

[8] Kyle W. Martin et al. "Compact Optical Atomic Clock Based on a Two-Photon Transition in Rubidium". In: *Phys. Rev. Applied* 9 (1 2018), p. 014019. DOI: 10.1103/PhysRevApplied.9.014019. URL: https://link.aps.org/doi/10.1103/PhysRevApplied.9.014019.

[9] L Hilico et al. "Metrological features of the rubidium two-photon standards of the BNM-LPTF and Kastler Brossel Laboratories". In: *The European Physical Journal-Applied Physics* 4.2 (1998), pp. 219–225.

[10] Y Millerioux et al. “Towards an accurate frequency standard at λ778 nm using a laser diode stabilized on a hyperfine component of the Doppler-free two-photon transitions in rubidium”. In: *Optics communications* 108.1-3 (1994), pp. 91–96.

[11] Zachary L. Newman et al. “High-performance, compact optical standard”. In: *Optics Letters* 46.18 (2021), p. 4702. ISSN: 0146-9592. DOI: 10.1364/ol.435603. arXiv: 2105.00610.

[12] C. Perrella et al. “High-resolution two-photon spectroscopy of rubidium within a confined geometry”. In: *Phys. Rev. A* 87 (1 2013), p. 013818. DOI: 10.1103/PhysRevA.87.013818. URL: https://link.aps.org/doi/10.1103/PhysRevA.87.013818.

[13] Heung-Ryoul Noh et al. “Modulation transfer spectroscopy for 87 Rb atoms: theory and experiment”. In: *Optics express* 19.23 (2011), pp. 23444–23452.

[14] Jon H Shirley. “Modulation transfer processes in optical heterodyne saturation spectroscopy”. In: *Optics Letters* 7.11 (1982), pp. 537–539.

[15] Edward A Whittaker, Manfred Gehrtz, and Gary C Bjorklund. “Residual amplitude modulation in laser electro-optic phase modulation”. In: *JOSA B* 2.8 (1985), pp. 1320–1326.

[16] David W Allan. “Statistics of atomic frequency standards”. In: *Proceedings of the IEEE* 54.2 (1966), pp. 221–230.

8 Appendix

8.1 Images of the Original Experimental Set Up

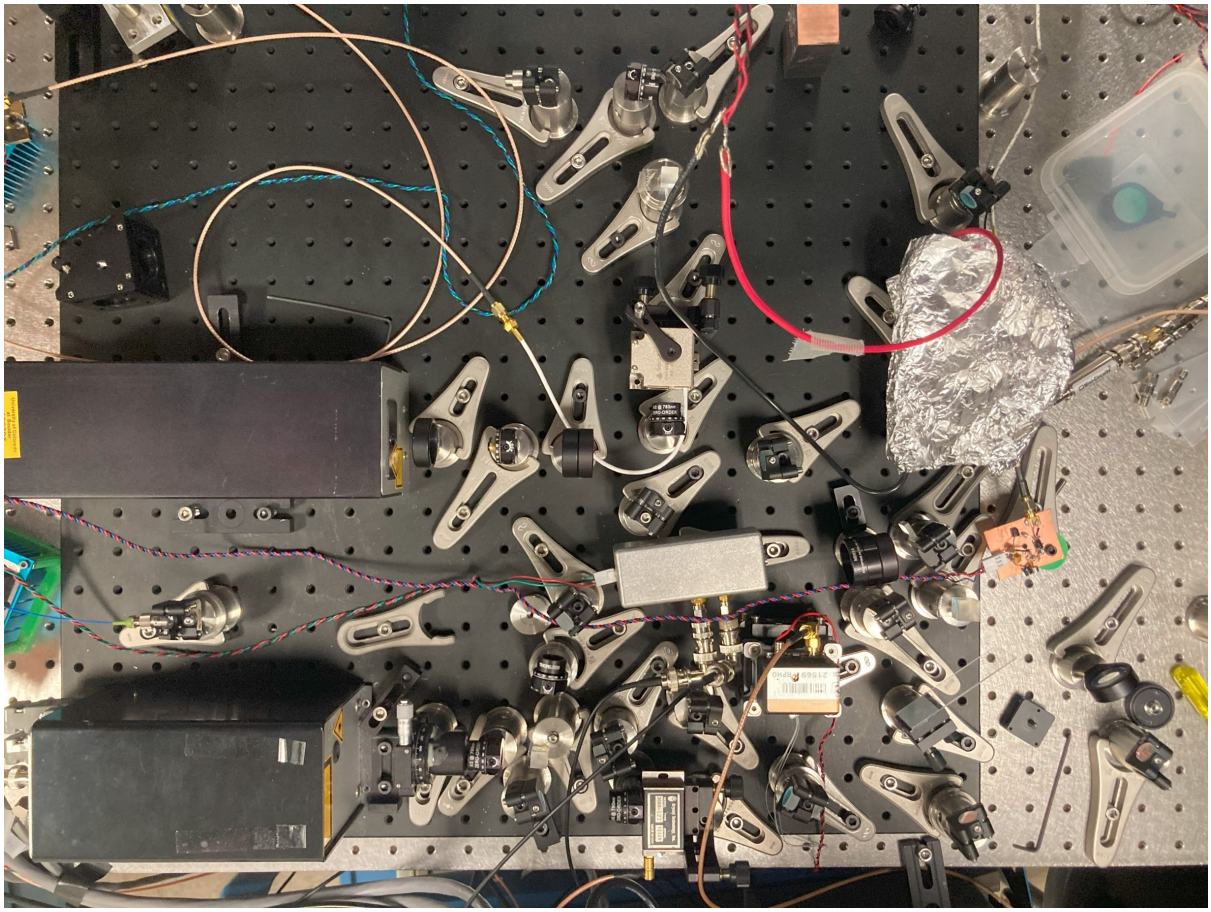

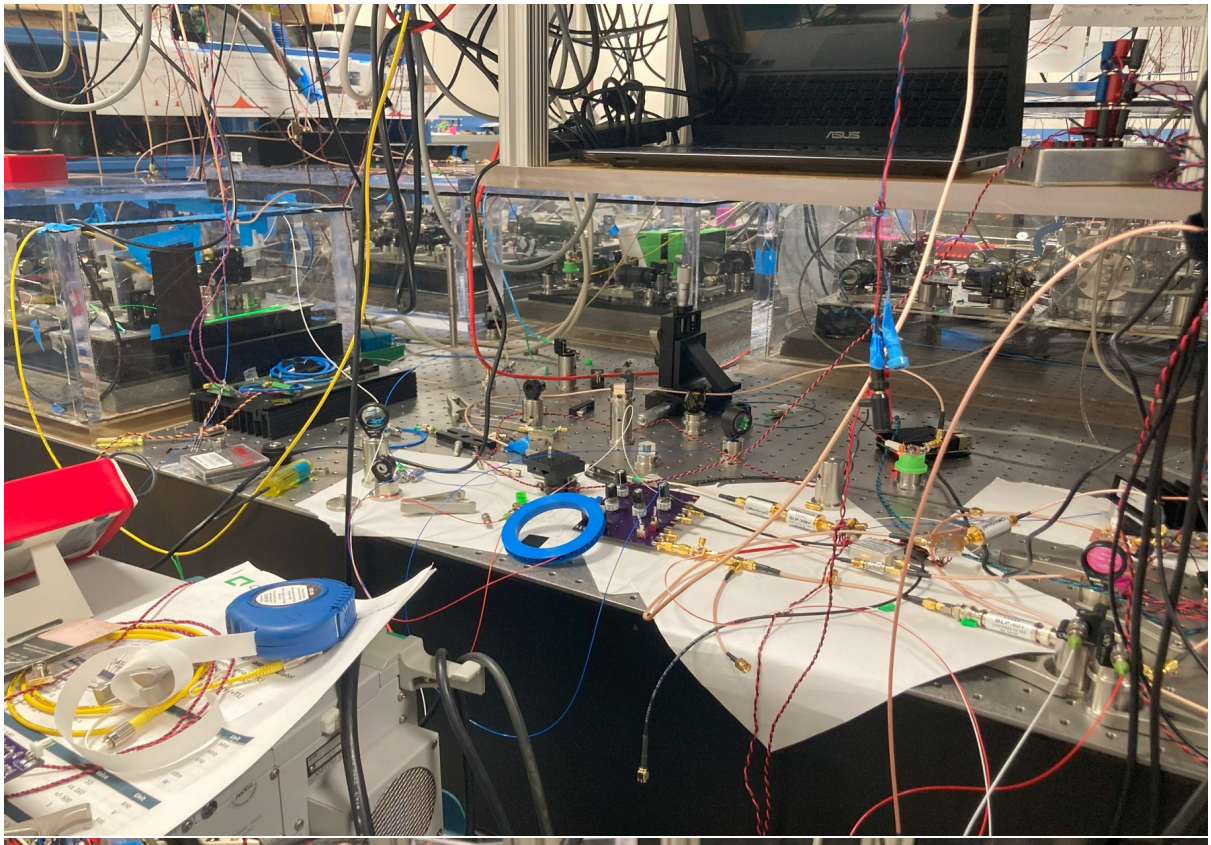

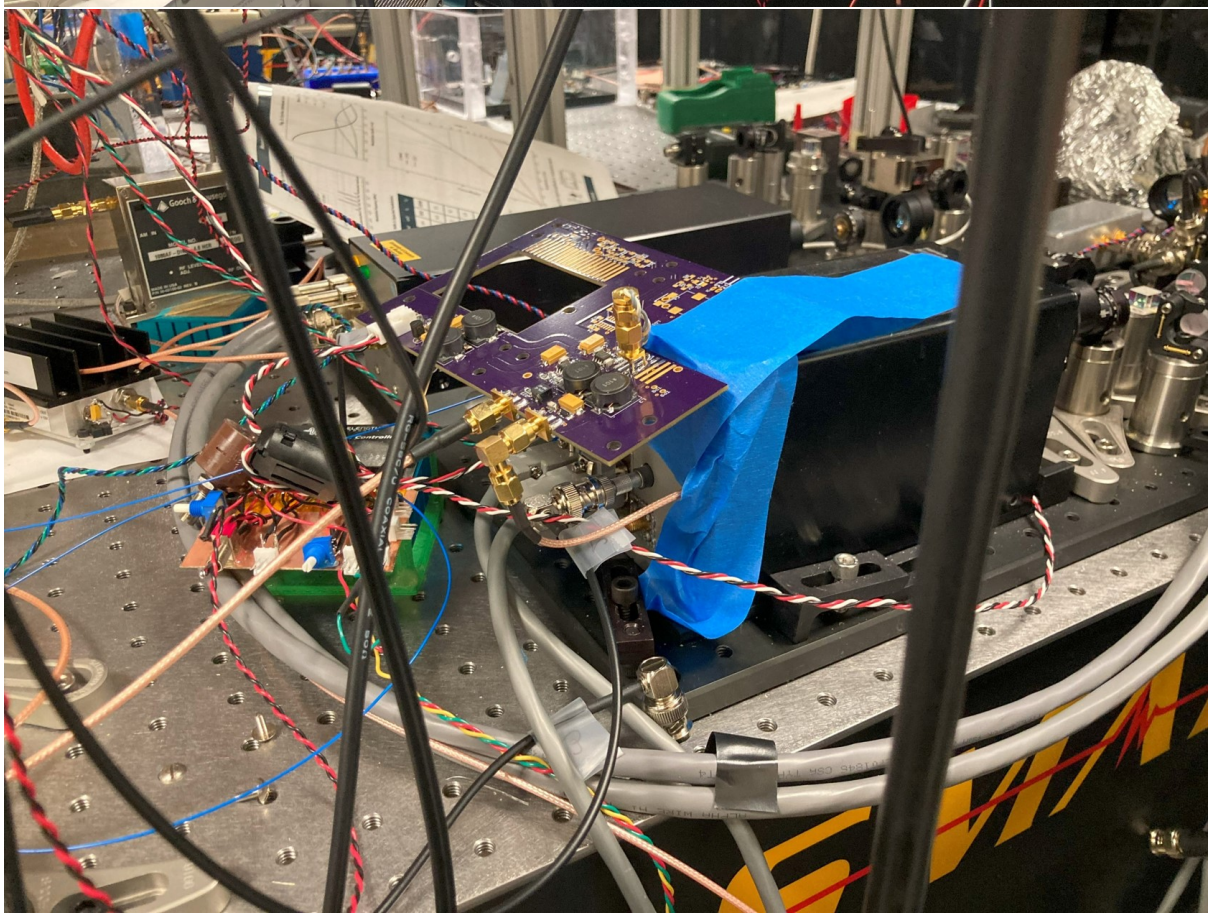

8.2 Images of Final Experimental Set Up

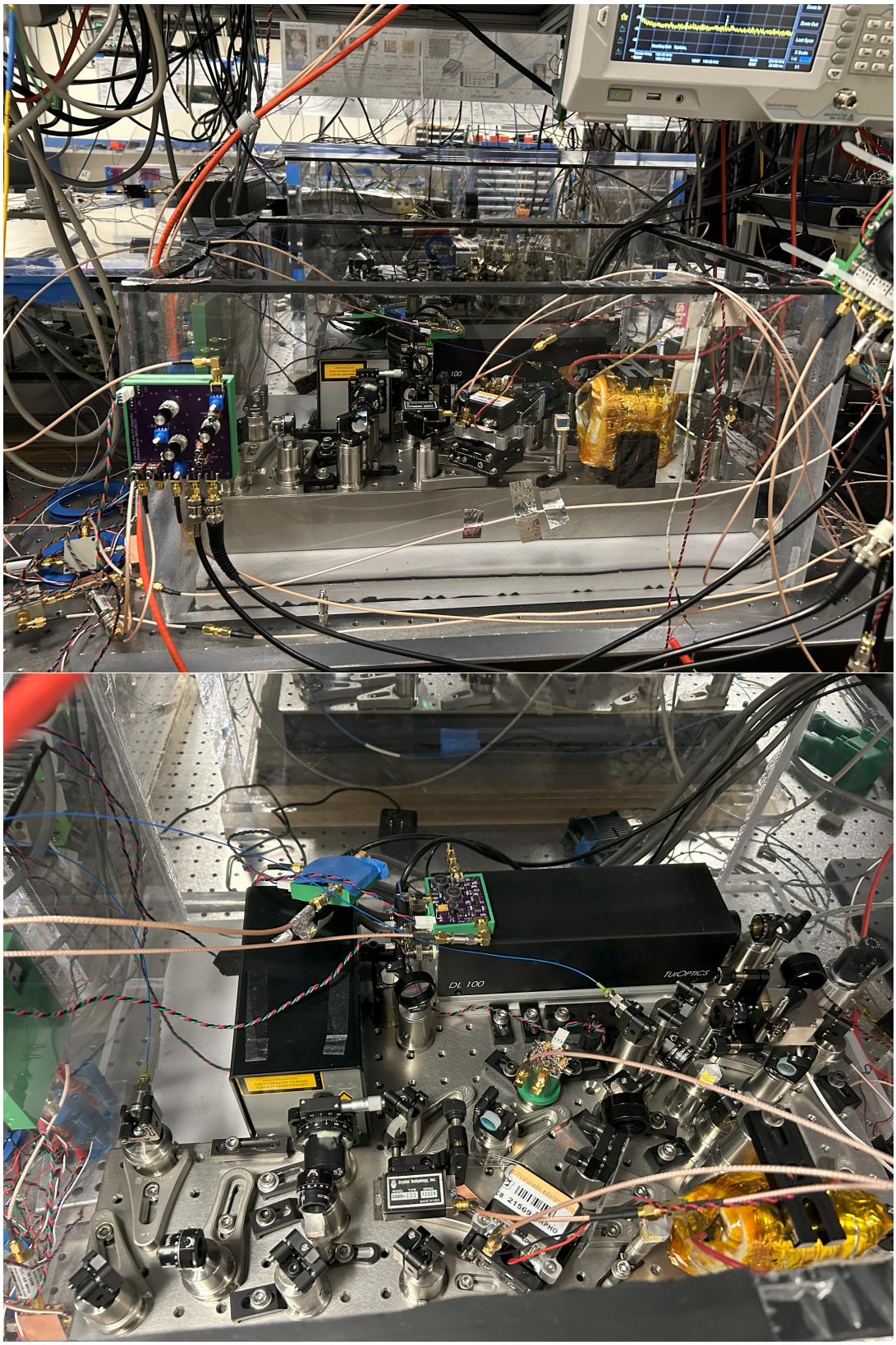

8.3 Generating Carrier Envelop Offset Frequency

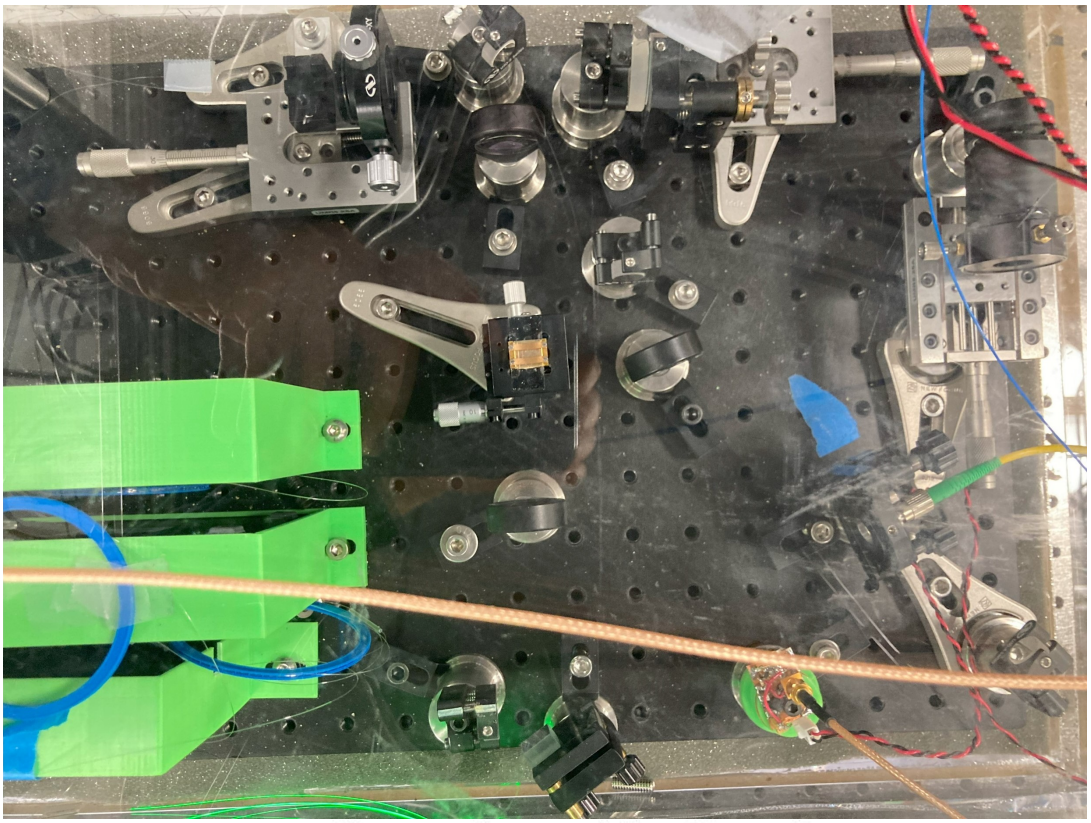

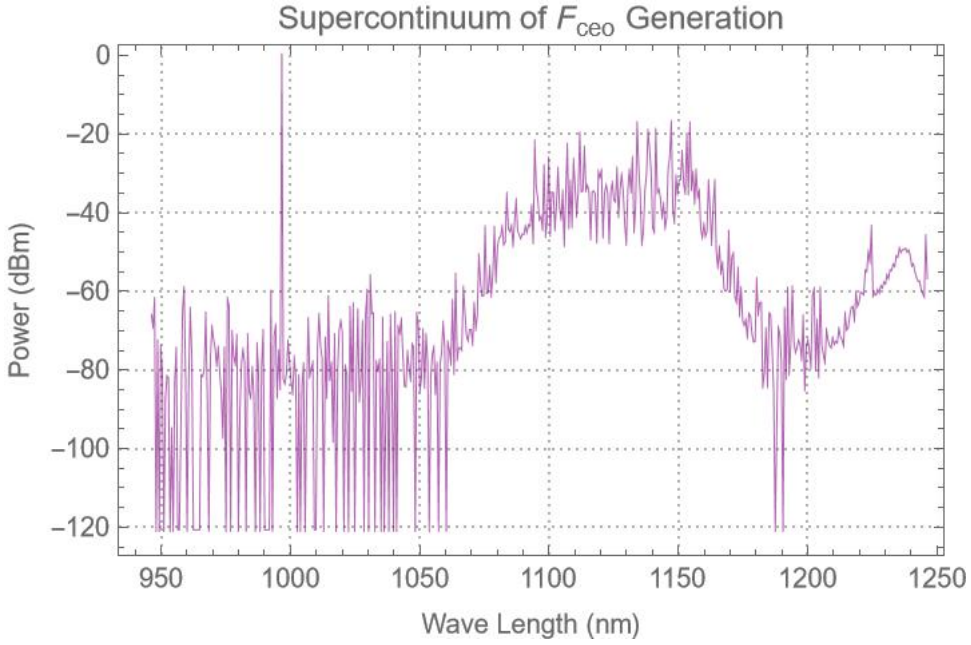

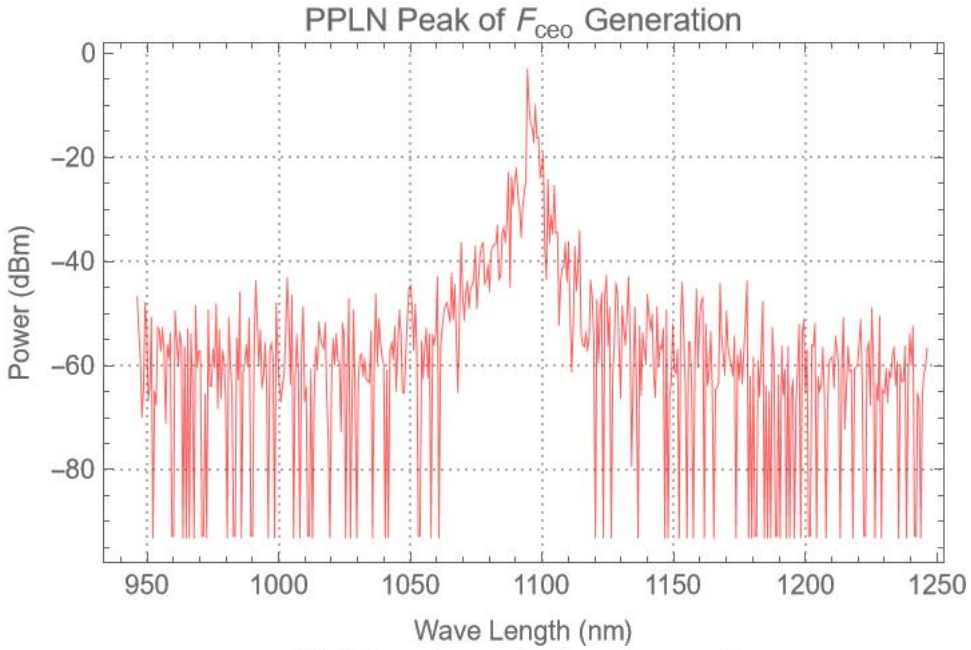
PPLN Peak of F_{ceo} Generation
0
−20
−40
−60
−80
Power (dBm)
950
1000
1050
1100
1150
1200
1250
Wave Length (nm)

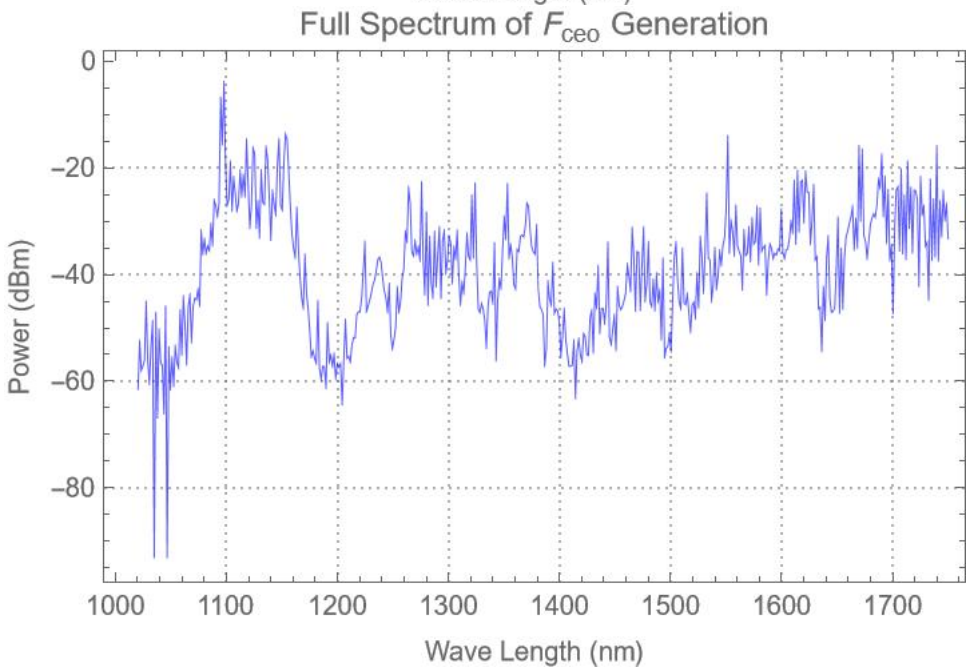
Full Spectrum of F_{ceo} Generation
0
−20
−40
−60
−80
Power (dBm)
1000
1100
1200
1300
1400
1500
1600
1700
Wave Length (nm)